Supporting information

Ultra-thin NiFeSe nanosheet as highly efficient bifunctional electrocatalyst for overall water splitting

Yu-Yang Sun [a, #], Mei-Yan Jiang [a, #], Lian-Kui Wu [a, b, *], Guang-Ya Hou [a], Yi-Ping Tang [a], Min Liu [c]

a. College of Materials Science and Engineering, Zhejiang University of Technology, Hangzhou 310014, China

b. School of Materials, Sun Yat-sen University, Guangzhou 510275, China

c. State Grid Zhejiang Electric Power Research Institute, Hangzhou 310014, China

#: These authors contributed equally to this work.

E-mail: wulk5@mail.sysu.edu.cn

Experimental

Chemicals

Ferrous sulfate heptahydrate ($FeSO_4 \cdot 7H_2O$, 99.0%) and selenium dioxide (SeO_2, 99.0%) were purchased from Shanghai Macklin Biochemical Technology Co. Ltd. Hydrochloric acid (HCl, 36.0%) was obtained from Hangzhou Shuang Lin chemical Co. Ltd. Potassium hydroxide (KOH, 85.0%) was obtained from Hangzhou Xiao Shan chemical reagent factory. Ethanol (CH_3CH_2OH, 99.7%) was purchased from Anhui An Te biochemistry company. All chemical reagents were used as received without further purification. Deionized (DI) water was used in all experiments.

Ni foam (NF, thickness: 1.5 mm, bulk density: 0.28 g cm^{-3}; number of pores per inch:

110) was purchased from Kunshan JiaYiSheng electronics. Co. Ltd. Before test, NF was immersed into 3.0 M HCl for 10 min, then washed with a plenty of running water and rinsed with DI water in an ultrasonic bath for 5 min, finally washed with ethanol for several times and blow-dried.

Fabrication of NiFeSe@NF

Typically, different amounts of $FeSO_4 \cdot 7H_2O$ (5, 10 mM) and SeO_2 (5, 10, 15 mM) were dissolved into 50 mL DI water. Then the obtained solution was transferred into a 100 mL Teflon-lined stainless steel autoclave and a piece of NF (1.0 cm × 2.5 cm) was added into the autoclave. Then the autoclave was maintained at 120 °C for 12 h, and cooled down to room temperature with the furnace. Finally, the specimen was removed out and rinsed thoroughly with DI water, ethanol and dried by warm air. Specimen labelled as $NiFe_{10}Se_{10}$@NF indicated that during the hydrothermal process, the amounts of $FeSO_4 \cdot 7H_2O$ and SeO_2 in the solution were both 10 mM.

Fabrication of Pt/C

In detail, 5.0 mg Pt/C powder was mixed with 200 μL isopropanol, 32 μL Nafion and 768 μL DI water (total 1 mL). After evenly dispersed by ultrasound, 200 μL suspension was dropped on a piece of NF (1.0 cm × 2.5 cm). The mass of the loaded active materials was about 1.0 mg cm^{-2}.

Physical-chemical Characterization

X-ray diffraction (XRD) patterns of the synthesized materials were recorded on a RIGAKU D/Max 2550 PC diffractometer equipped with Cu Kα radiation (λ=1.54059 Å) at 40 kV and 30 mA. The morphology and composition of the electrodes were

characterized by field emission scan electron microscopy (FE-SEM, Carl Zeiss Supra 55, operated at 15 kV) equipped with energy dispersive X-ray spectra (EDS) microanalysis (Oxford EDS Inca Energy Coater 300) and atomic force microscopy (AFM, Bruker Dismension Icon 3 atomic force micro-scope). The transmission electron microscopy (TEM) and high-resolution TEM (HR-TEM) images were acquired on a Tecnai G2 F30 (Philips-FEI, Co. Ltd) instrument. The surface chemical state and composition of the active materials were investigated by X-ray Photoelectron Spectroscopy (XPS) (Kratos AXIS Ultra DLD) using Al Kα excitation.

Electrochemical measurements

All electrochemical measurements were performed on a CS 310H electrochemical workstation at 25 ± 1 °C in 1.0 M KOH solution. The measurement was carried out in a three-electrode compartment. NiFeSe@NF was used as the working electrode. An Ag/AgCl was served as the reference electrode and a Pt foil with exposed area of 4.0 cm^2 was used as the counter electrode. Potentials *vs.* RHE are calculated using the Nernst equation, $E_{RHE} = E_{Ag/AgCl} + 0.059 \times pH + 0.197$ V. Linear sweep voltammetry (LSV) measurements were carried out with scan rate of 1.0 mV s^{-1}. The polarization curves were IR-corrected as following: $E = E_{apply} - iR$. Cyclic voltammetry (CV) tests were conducted to probe the electrochemical double layer capacitance of samples at non-faradaic potential region. In detail, a series of CV measurements were performed from 0.1 to 0.15 V and -0.3 to 0.35 V *vs.* Ag/AgCl towards OER and HER, respectively, at various scan rates from 20 to 100 mV s^{-1}. By plotting the difference of current density (ΔJ) between the anodic and cathodic sweeps ($J_{anodic} - J_{cathodic}$) against the scan rate, a

linear trend was observed. The slope of the fitting line is equal to twice the geometric double layer capacitance (C_{dl}), which is proportional to the effective electrode surface area of the materials. Electrochemical impedance spectroscopy (EIS) measurements were carried out at 1.5 V and -1.2 V *vs.* Ag/AgCl towards OER and HER, respectively, over the frequency range from 100 kHz to 10 mHz with the AC amplitude of 5 mV. Chronopotentiometric measurements were tested at 10 mA cm^{-2} for 10 h towards OER and HER.

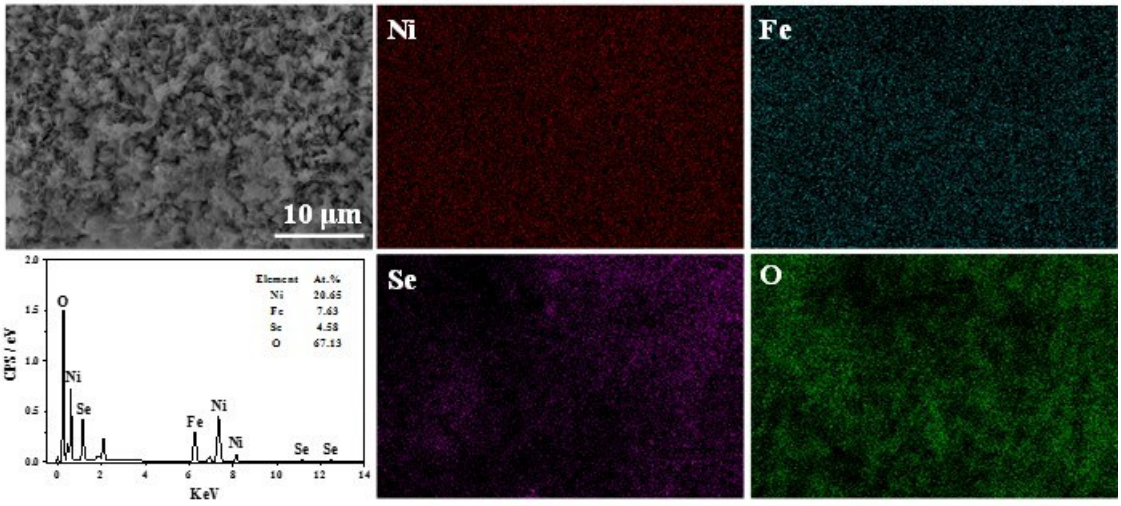

Fig. S1 SEM image, EDS spectra and corresponding elemental mapping images of $NiFe_{10}Se_{10}$@NF.

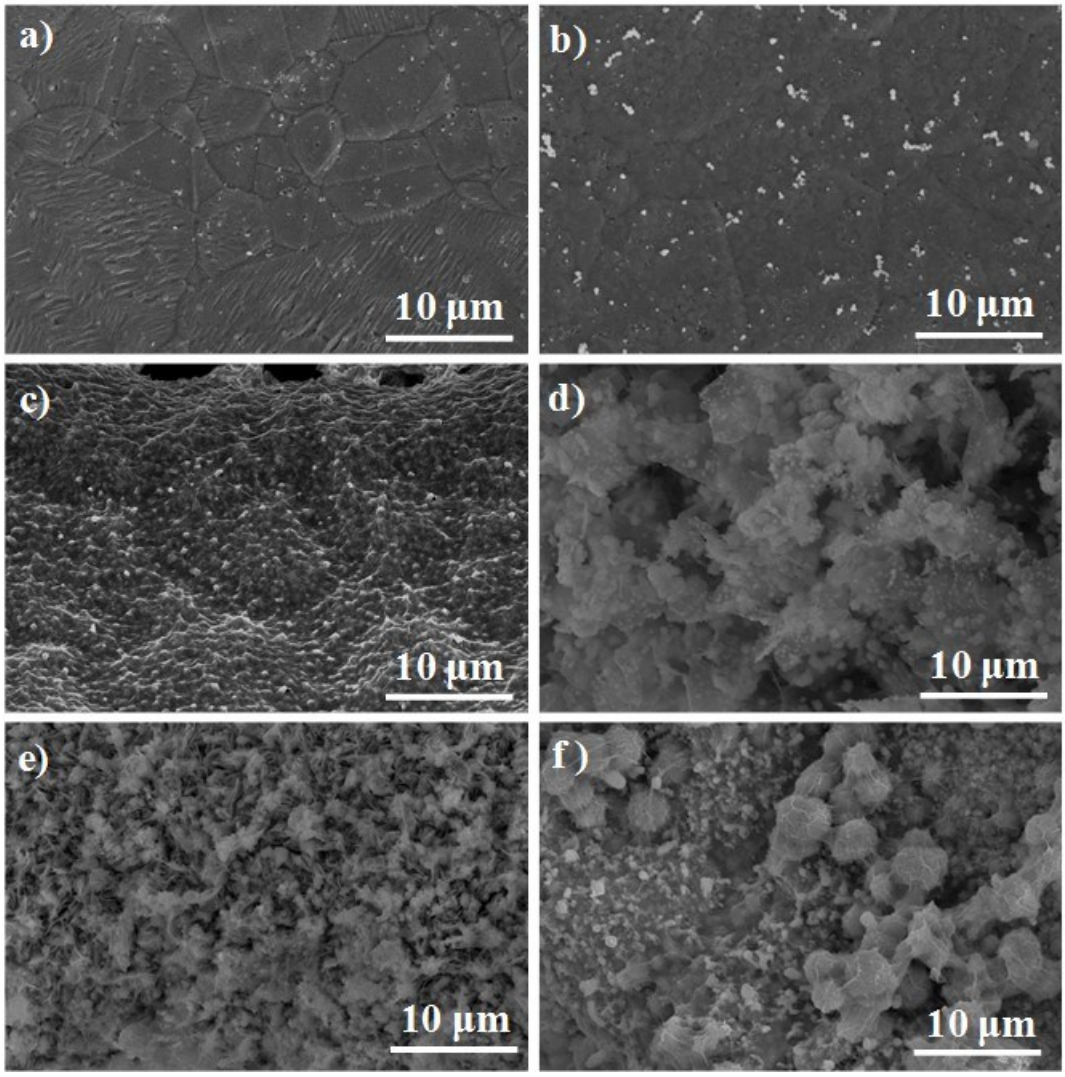

Fig. S2 SEM images of $NiFe_{10}$@NF (a), $NiSe_{10}$@NF (b), $NiFe_5Se_{10}$@NF (c), $NiFe_{10}Se_5$@NF (d), $NiFe_{10}Se_{10}$@NF (e) and $NiFe_{10}Se_{15}$@NF (f).

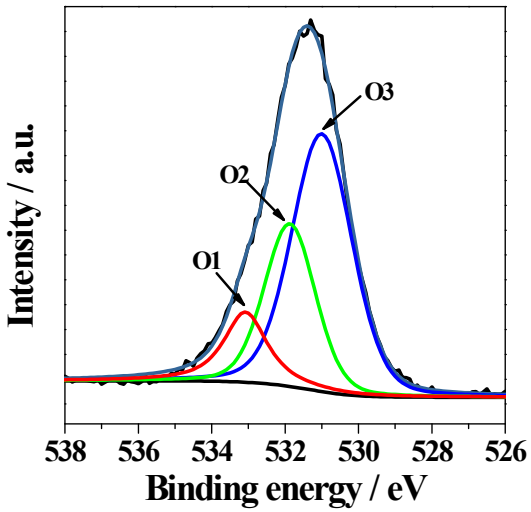

Fig. S3 High-resolution XPS spectra of O 1s of $NiFe_{10}Se_{10}$@NF.

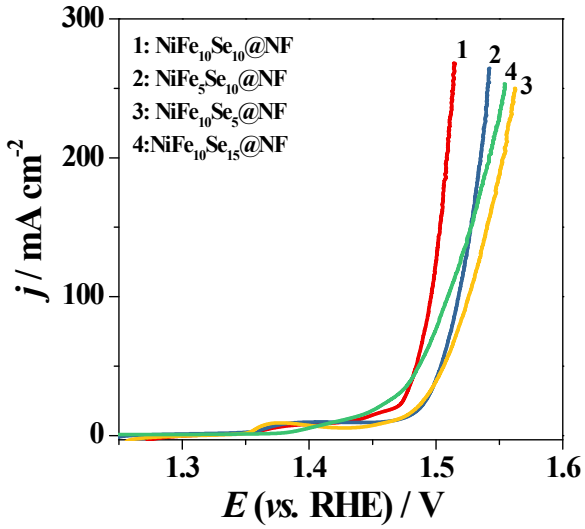

Fig. S4 LSV curves towards OER of $NiFe_{10}Se_{10}$@NF (1), $NiFe_5Se_{10}$@NF (2), $NiFe_{10}Se_5$@NF (3) and $NiFe_{10}Se_{15}$@NF (4).

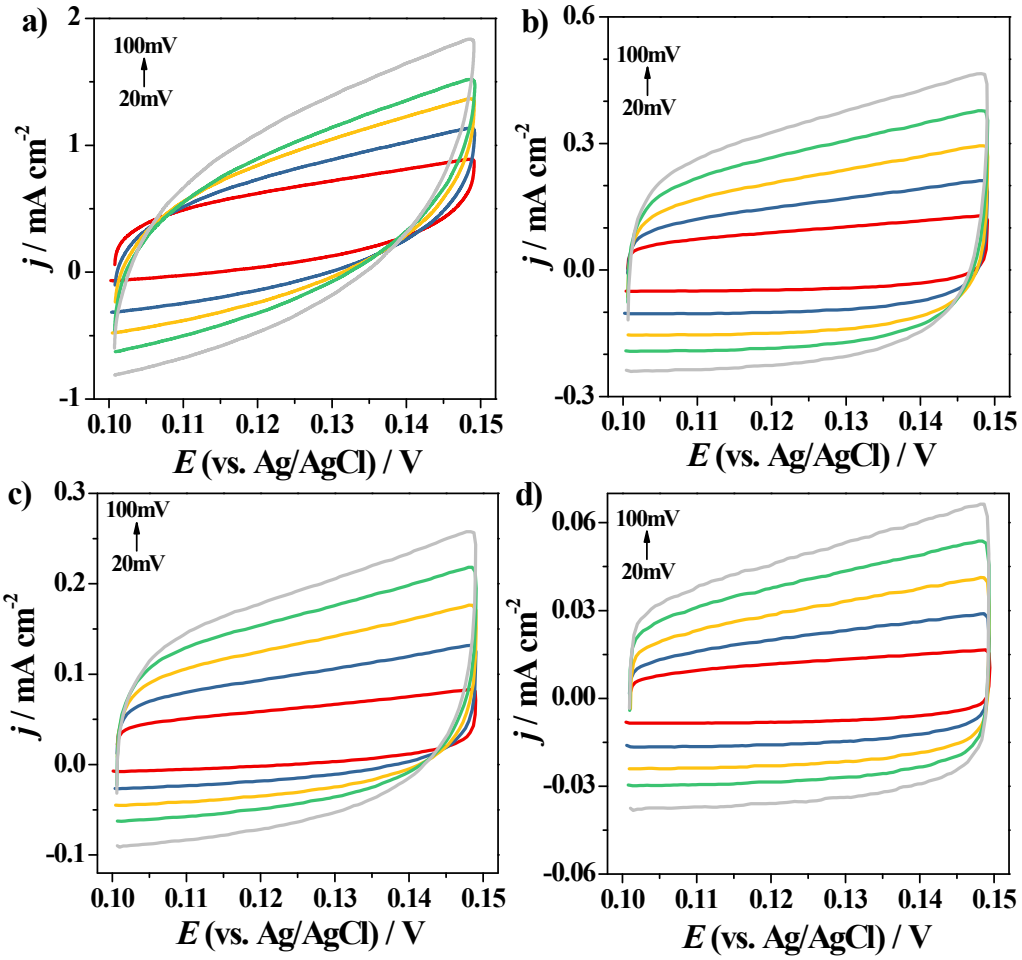

Fig. S5 CV curves (OER) in the double layer region with various scan rates from 20 to 100 mV s^{-1} for $NiFe_{10}Se_{10}$@NF (a), $NiSe_{10}$@NF (b), $NiFe_{10}$@NF (c) and NF (d) and the corresponding linear fitting of the capacitive density versus scan rates (e).

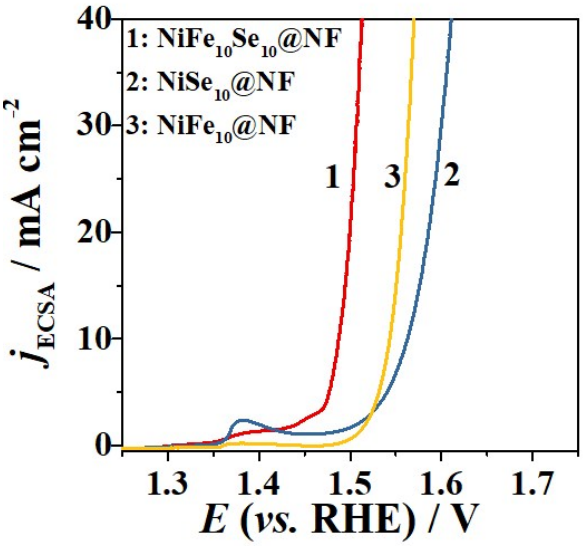

Fig. S6 The LSV curves in Fig. 6a normalized to the ECSA.

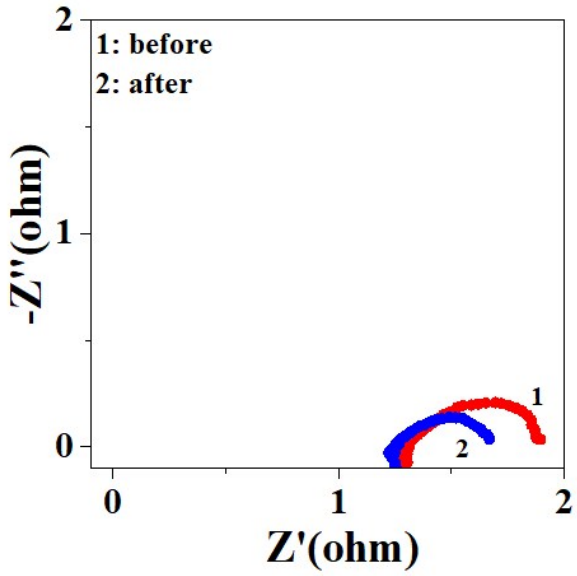

Fig. S7 Nyquist plots of the $NiFe_{10}Se_{10}$@NF before (1) and after (2) OER chronopotentiometric test for 10h.

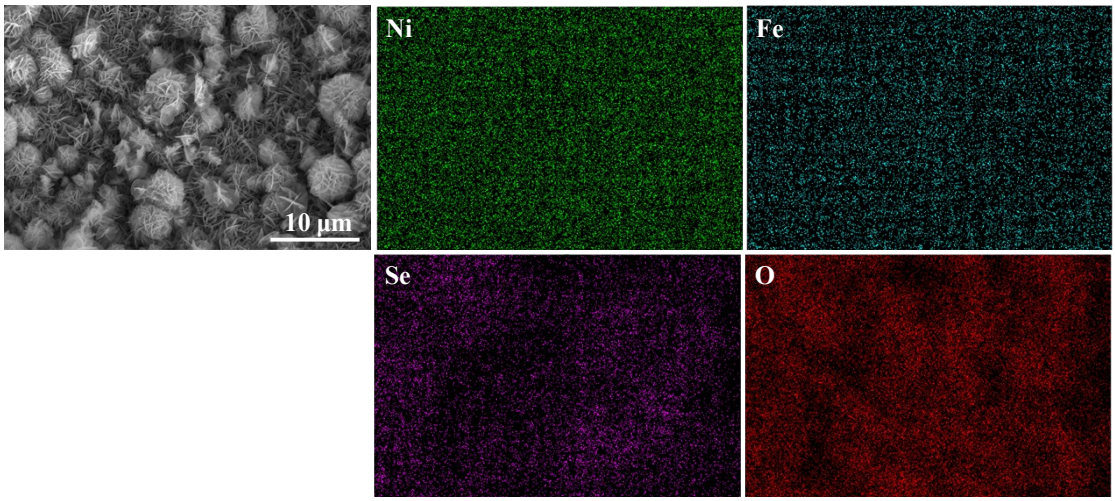

Fig. S8 SEM image and corresponding elemental mapping images of $NiFe_{10}Se_{10}$@NF after OER chronopotentiometric test for 10 h.

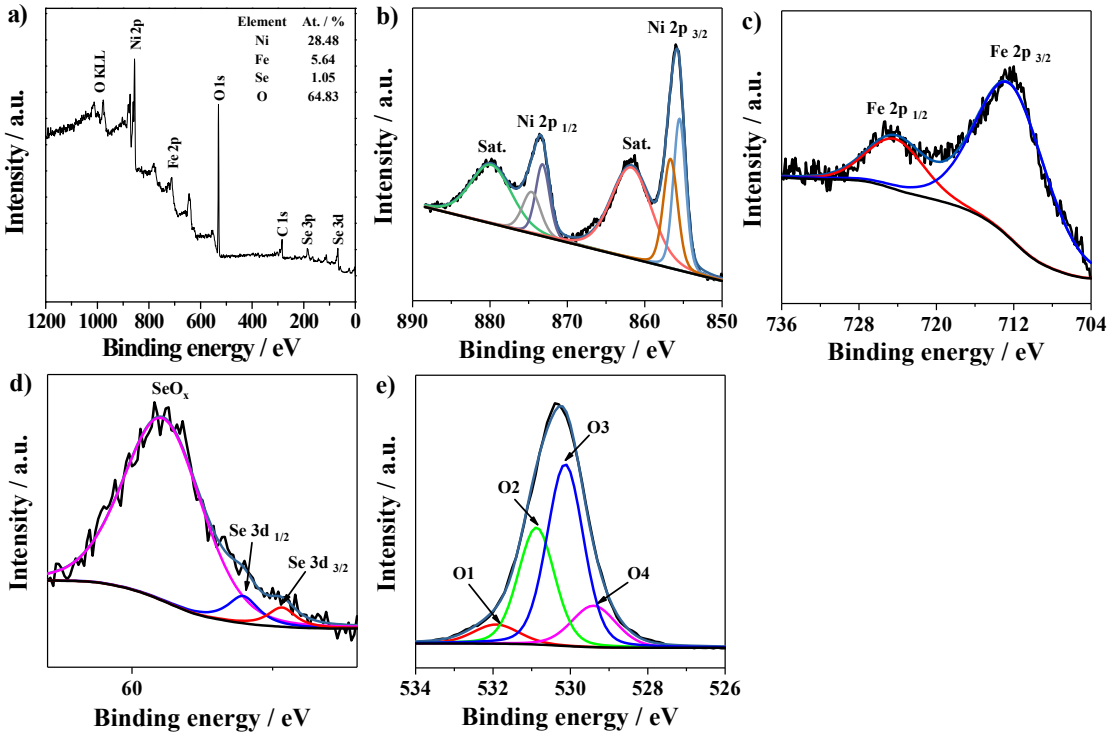

Fig. S9 Survey XPS spectra (a) and high-resolution XPS spectra of Ni 2p (b), Fe 2p (c), Se 3d (d), and O 1s (e) of $NiFe_{10}Se_{10}$@NF after OER stability test for 10 h.

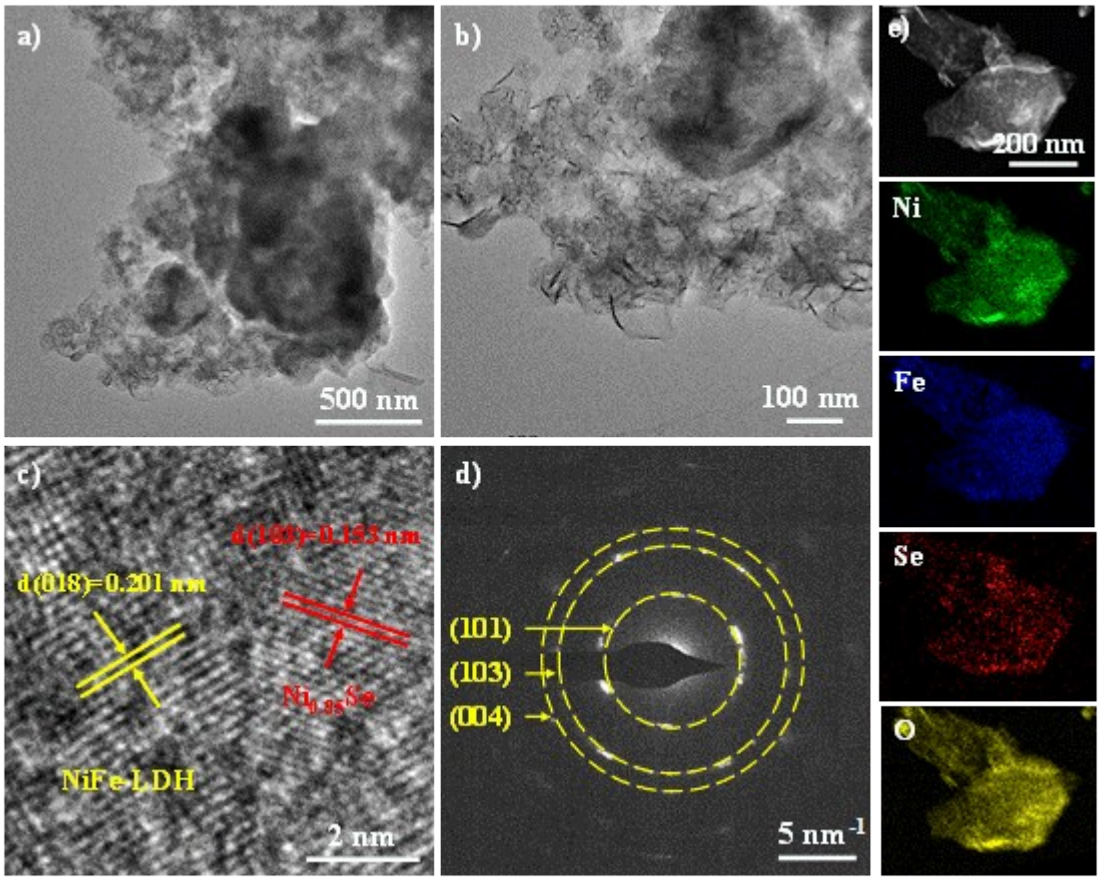

Fig. S10 Low (a, b) and high (c) resolution TEM images, SAED pattern (d), HAADF image and corresponding STEM-EDS elemental mapping (Ni, Se, and O) (e) of the $NiFe_{10}Se_{10}$@NF after OER stability test.

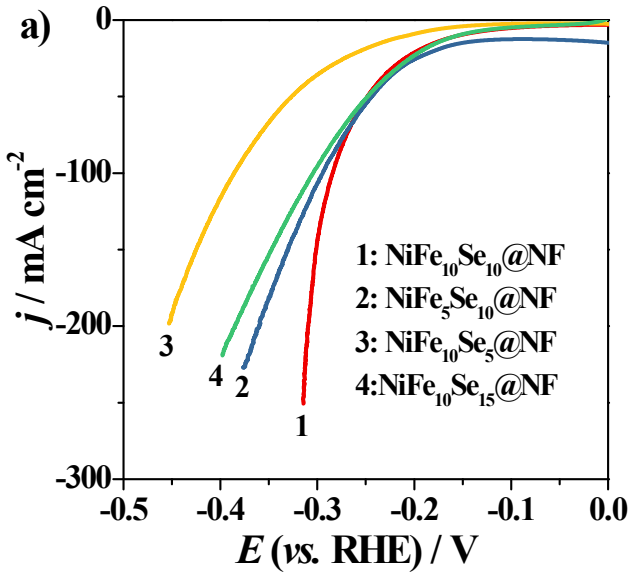

Fig. S11 LSV curves towards HER of $NiFe_{10}Se_{10}$@NF(1), $NiFe_5Se_{10}$@NF(2), $NiFe_{10}Se_5$@NF(3) and $NiFe_{10}Se_{15}$@NF(4).

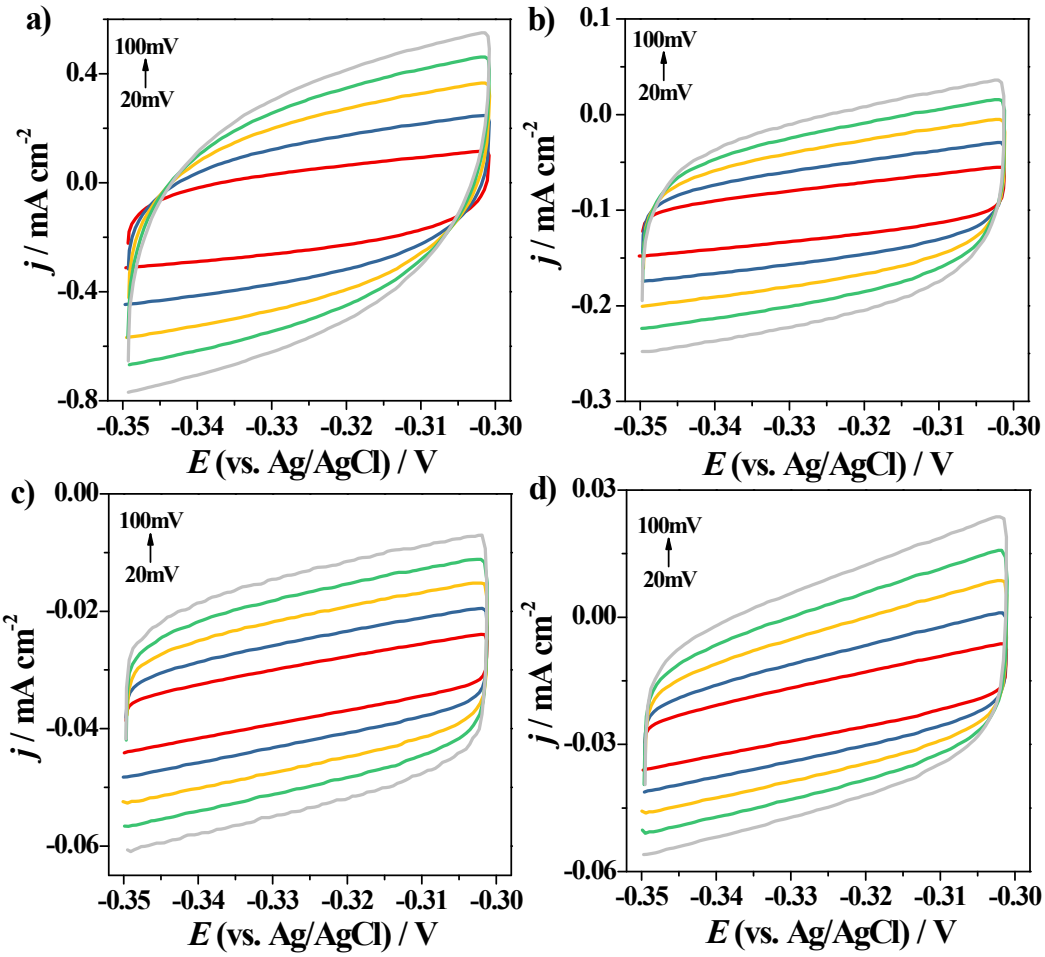

Fig. S12 CV curves (HER) in the double layer region with various scan rates from 20 to 100 mV s^{-1} for$NiFe_{10}Se_{10}$@NF(a), $NiSe_{10}$@NF(b), $NiFe_{10}$@NF(c) and NF(d) and the corresponding linear fitting of the capacitive density versus scan rates(d).

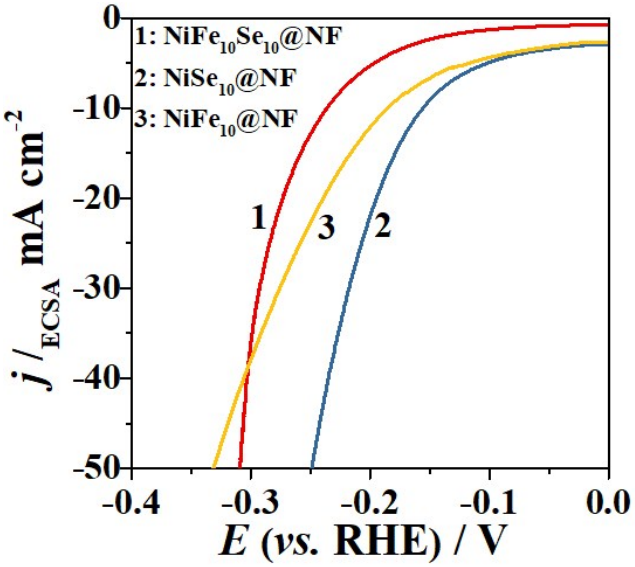

Fig. S13 The LSV curves in Fig. 7a normalized to the ECSA.

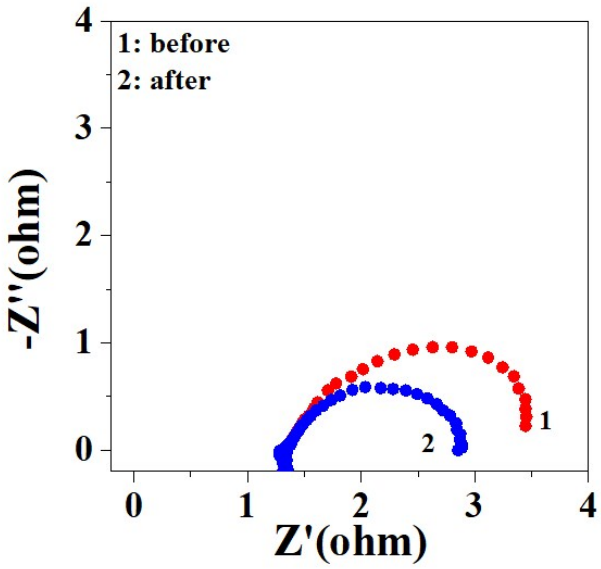

Fig. S14 Nyquist plots of the $NiFe_{10}Se_{10}$@NF before (1) and after (2) HER chronopotentiometric test for 10h.

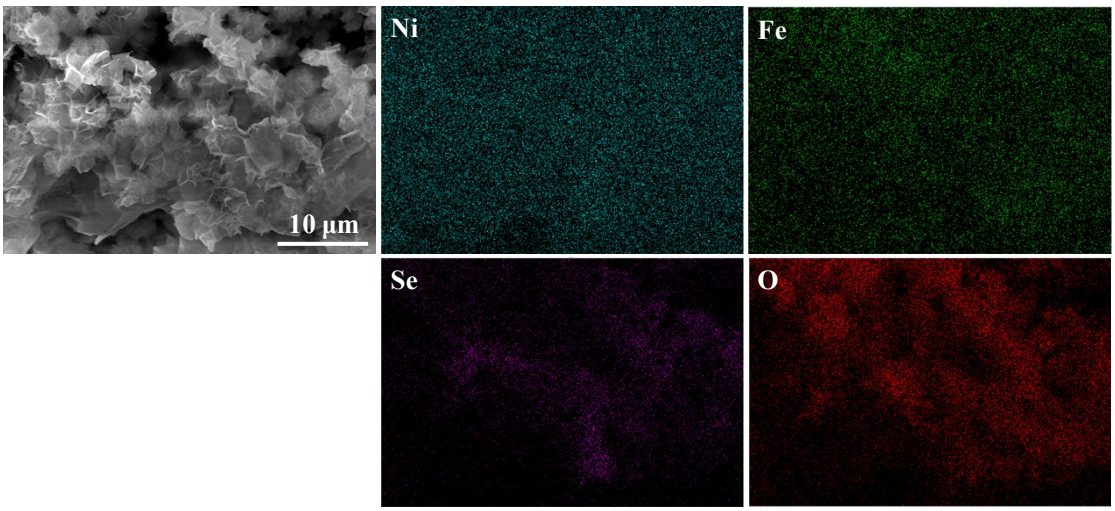

Fig. S15 The SEM image and corresponding elemental mapping images of $NiFe_{10}Se_{10}$@NF after HER chronopotentiometric test.

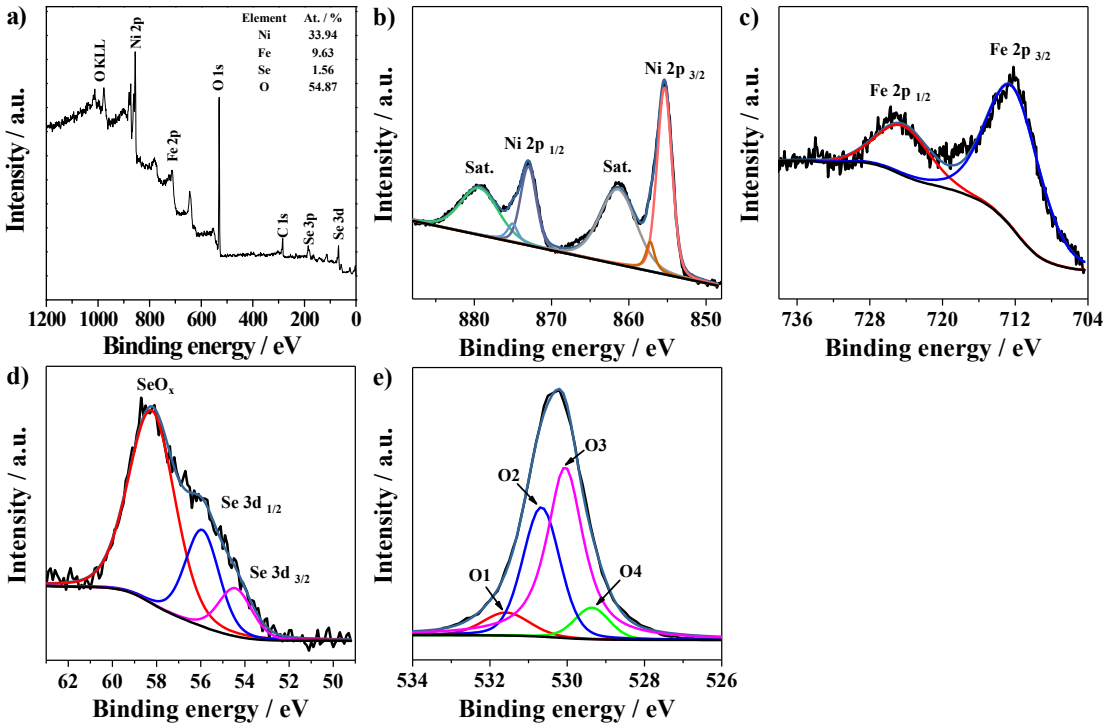

Fig. S16 Survey XPS spectra (a) and high-resolution XPS spectra of Ni 2p (b), Fe 2p (c), Se 3d (d) and O 1s (e) of $NiFe_{10}Se_{10}$@NF after HER stability test.

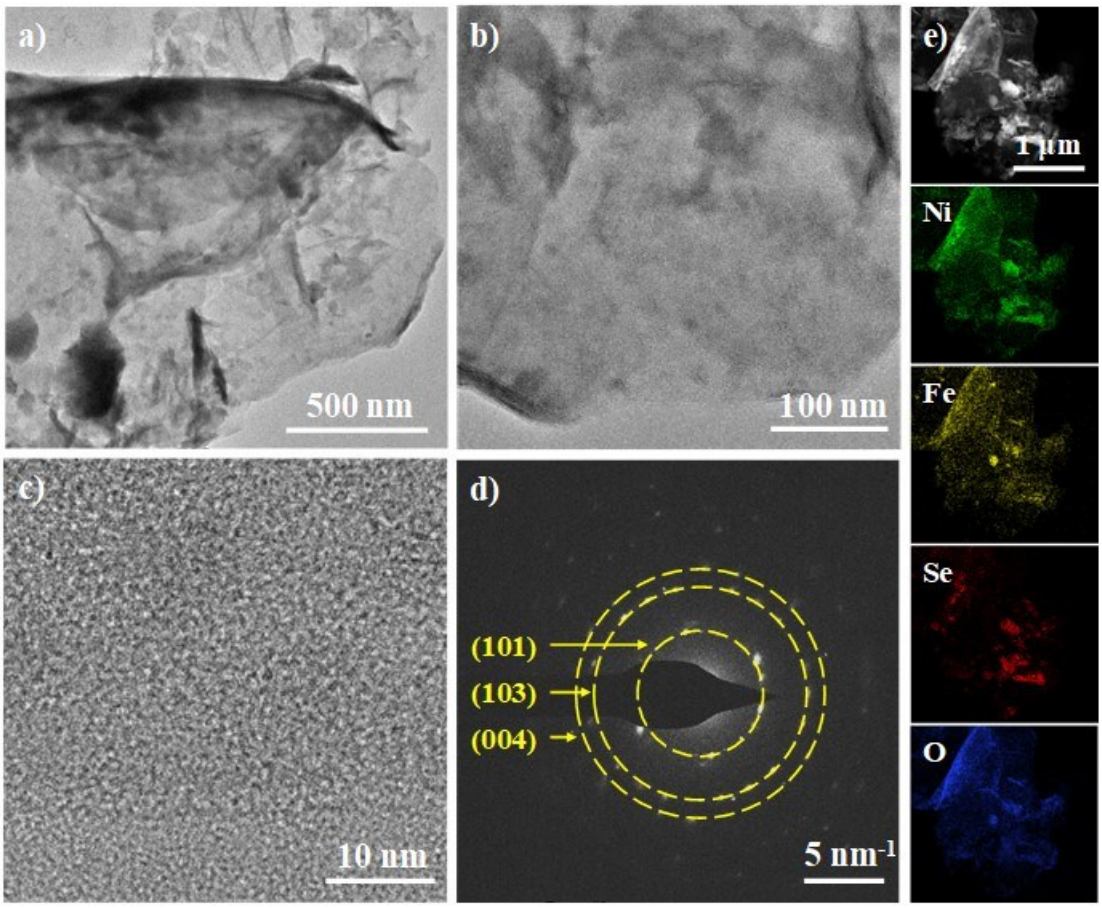

Fig. S17 Low (a, b) and high (c) resolution TEM images, SAED pattern (d), HAADF image and corresponding STEM-EDS elemental mapping (Ni, Se, and O) (e) of the $NiFe_{10}Se_{10}$@NF after HER stability test.

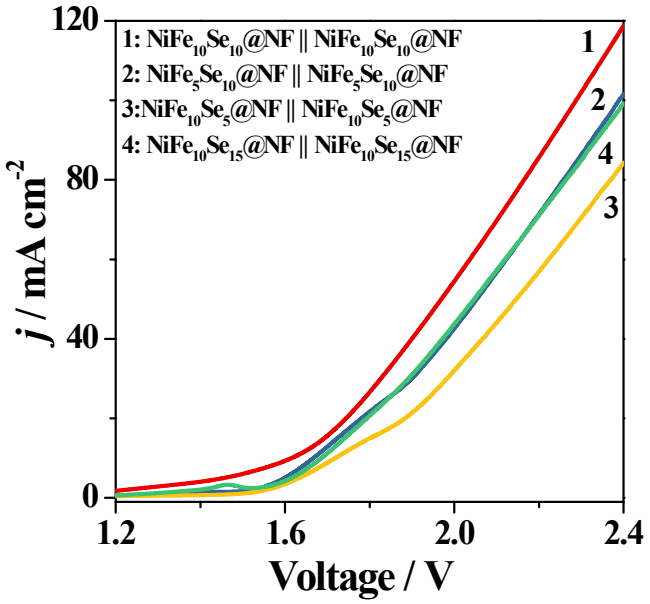

Fig. S18 LSV curves of water electrolysis for $NiFe_{10}Se_{10}$@NF || $NiFe_{10}Se_{10}$@NF (1), $NiFe_5Se_{10}$@NF || $NiFe_5Se_{10}$@NF (2), $NiFe_{10}Se_5$@NF || $NiFe_{10}Se_5$@NF (3) and $NiFe_{10}Se_{15}$@NF || $NiFe_{10}Se_{15}$@NF (4) in a two-electrode configuration.

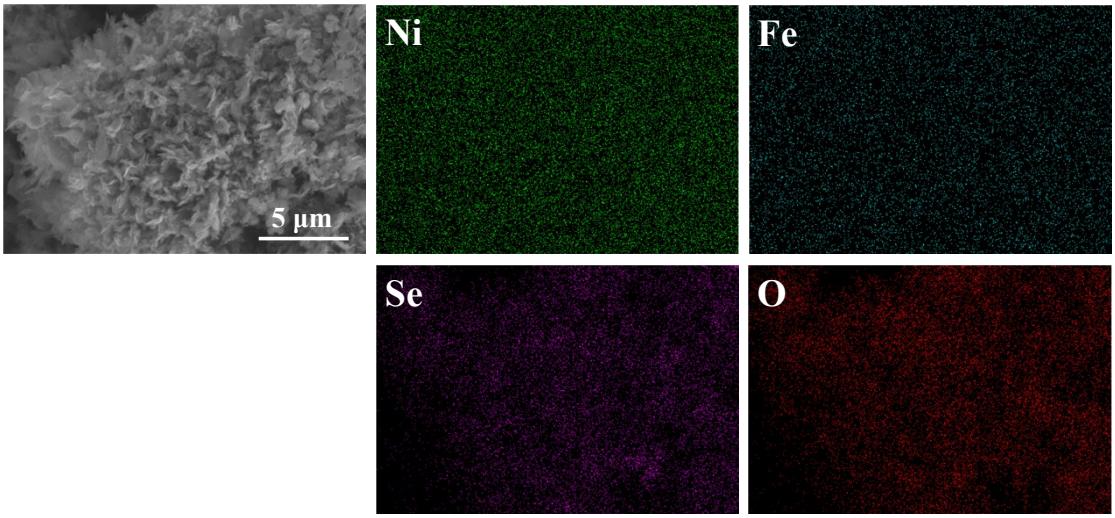

Fig. S19 The SEM image and corresponding elemental mapping images of $NiFe_{10}Se_{10}$@NF (anode) after overall water stability test.

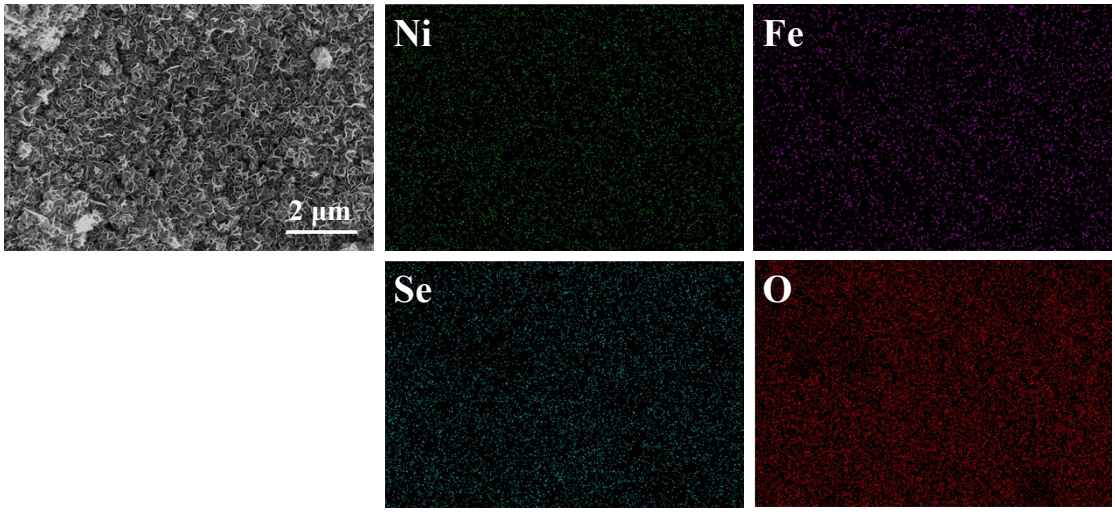

Fig. S20 The SEM image and corresponding elemental mapping images of $NiFe_{10}Se_{10}$@NF (cathode) after overall water stability test.

Table S1 Comparison of alkaline OER performance for $NiFe_{10}Se_{10}$@NF with other nickel-based selenide Catalyst Electrocatalysts.

Nickel-based selenide Catalyst	Tafel slope / mV dec^{-1}	Overpotential / mV (j = 10 mA cm^{-2})	Ref.
$NiFe_{10}Se_{10}$@NF	40	199	This work
Se-(NiCo)S/OH	33.9	155	[1]
NiSe–PANI	145.4	180	[2]
$NiCoSe_2$/NF	97	183	[3]
$Ni_xFe_{1-x}Se_2$-DO	28	195	[4]
$(Ni,Co)Se_2$/NiFe-LDH	61	205	[5]
$NiCoSe_2$-x/N-doped C	75	215	[6]
Ni-Fe-$Se_{1:1}$-180	36	216	[7] a
$(Ni,Fe)_3Se_4$	41	225	[8]
$(Ni_{0.77}Fe_{0.23})Se_2$/CC	69	228	[9]
$Ni_{0.5}Fe_{0.5}Se_2$	34.7	235	[10]
$(Ni_{0.75}Fe_{0.25})Se_2$	47.2	255	[11]
$(Ni,Co)Se_2$	74	256	[12]
$Ni_{0.7}Co_{0.3}Se_2$	42.3	258	[13]
Fe–NiSe/NF	48	261	[14]
$NiCoSe_2$/NF	61.2	274	[15]
$(Co,Ni)Se_2$@NiFe LDH	75	277	[16]

Note: DO: the selenide-derived oxide.

a: The data were chosen from the hydrothermal temperature for 180℃.

Table S2 Comparison of alkaline HER performance for $NiFe_{10}Se_{10}$@NF with other nickel-based selenide Catalyst Electrocatalysts.

Nickel-based selenide Catalyst	**Tafel slope / mV dec^{-1}**	**Overpotential / mV (j = 10 mA cm^{-2})**	**Ref.**
$NiFe_{10}Se_{10}$@NF	129.3	154	This work
$NiFe_{10}Se_{10}$@NF- after stablility test		86	This work
$NiSe/Ni_3Se_2$/NF-12	101.2	92	[17]
Se-$(NiCo)S_x/(OH)_x$	87.3	103	[1]
$Ni_{0.75}Fe_{0.25}Se_2$	86.5	117	[18]
NiSe/NF	76	160	[19]
NiFe-Se/C	94	160	[20]
$Ni_{0.54}W_{0.26}Se$	74	162	[21]
$(Ni,Co)_{0.85}Se$	115.66	169	[22]
NiSe/NF(ethonal)	103	170.5	[23]
$Co/(NiCo)Se_2$	39.8	190	[24]
$NiSe_2$	72.11	198	[25]
$Ni_{0.75}Se$	86	233	[26]
Y-S Ni-Co-Se/CFP	72	250	[27]
$NiSe_2$	35	269	[28]

Table S3 Comparison of alkaline overall water splitting performance for $NiFe_{10}Se_{10}$@NF with other nickel-based selenide Catalyst.

Nickel-based selenide Catalyst	**Cell Votage / V (j = 10 mA cm^{-2})**	**Ref.**
$NiFe_{10}Se_{10}$@NF	1.61	This work
(Ni,Co)Se_2/C-HRD	1.58	[29]
(Ni,Co)Se_2-GA	1.6	[30]
Se-(NiCo)S_x/$(OH)_x$	1.6	[1]
NiSe/Ni_3Se_2/NF-12	1.6	[17]
$Ni_{0.75}Fe_{0.25}Se_2$	1.61	[18]
NiSe-$Ni_{0.85}$Se/CP	1.62	[31]
$(Ni,Co)_{0.85}$Se	1.65	[22]
$Co_{0.85}$Se/NiFe-LDH	1.67	[19]
NiFe-Se/C	1.68	[20]
$Ni_{0.5}$Se||$Ni_{0.75}$Se	1.73	[26]

Note: GA: graphene aerogel; HRD: hollow rhombic dodecahedra.

Reference:

[1] C. Hu, L. Zhang, Z.-J. Zhao, A. Li, X. Chang, J. Gong, Synergism of Geometric Construction and Electronic Regulation: 3D Se-(NiCo)S_x/$(OH)_x$ Nanosheets for Highly Efficient Overall Water Splitting, Adv Mater, 30 (2018) 1705538.

[2] P.F. Liu, L. Zhang, L.R. Zheng, H.G. Yang, Surface engineering of nickel selenide for an enhanced intrinsic overall water splitting ability, Materials Chemistry Frontiers, 2 (2018) 1725-1731.

[3] K. Akbar, J.H. Jeon, M. Kim, J. Jeong, Y. Yi, S.-H. Chun, Bifunctional Electrodeposited 3D $NiCoSe_2$/Nickle Foam Electrocatalysts for Its Applications in Enhanced Oxygen Evolution Reaction and for Hydrazine Oxidation, ACS Sustain Chem Eng, 6 (2018) 7735-7742.

[4] X. Xu, F. Song, X. Hu, A nickel iron diselenide-derived efficient oxygen-evolution catalyst, Nat Commun, 7 (2016) 12324.

[5] X. Li, H. Wu, Y. Wu, Z. Kou, S.J. Pennycook, J. Wang, NiFe Layered Double-Hydroxide Nanosheets on a Cactuslike (Ni,Co)Se_2 Support for Water Oxidation, ACS Appl Nano Mater, 2 (2018) 325-333.

[6] J. Li, M. Wan, T. Li, H. Zhu, Z. Zhao, Z. Wang, W. Wu, M. Du, $NiCoSe_{2-x}$/N-doped C mushroom-like core/shell nanorods on N-doped carbon fiber for efficiently electrocatalyzed overall water splitting, Electrochim Acta, 272 (2018) 161-168.

[7] C. Xuan, K. Xia, W. Lei, W. Xia, W. Xiao, L. Chen, H.L. Xin, D. Wang, Composition-dependent electrocatalytic activities of NiFe-based selenides for the oxygen evolution reaction, Electrochim Acta, 291 (2018) 64-72.

[8] J. Du, Z. Zou, C. Liu, C. Xu, Hierarchical Fe-doped Ni_3Se_4 ultrathin nanosheets as an efficient electrocatalyst for oxygen evolution reaction, Nanoscale, 10 (2018) 5163-5170.

[9] Q. Yan, P. Yan, T. Wei, G. Wang, K. Cheng, K. Ye, K. Zhu, J. Yan, D. Cao, Y. Li, A highly efficient and durable water splitting system: platinum sub-nanocluster functionalized nickel–iron layered double hydroxide as the cathode and hierarchical nickel–iron selenide as the anode, J Mater Chem A, 7 (2019) 2831-2837.

[10] Y. Du, G. Cheng, W. Luo, $NiSe_2$/$FeSe_2$ nanodendrites: a highly efficient electrocatalyst for oxygen evolution reaction, Catal. Sci. Technol., 7 (2017) 4604-4608.

[11] Z. Wang, J. Li, X. Tian, X. Wang, Y. Yu, K.A. Owusu, L. He, L. Mai, Porous Nickel-Iron Selenide Nanosheets as Highly Efficient Electrocatalysts for Oxygen Evolution Reaction, ACS Appl Mater Interfaces, 8 (2016) 19386-19392.

[12] W. Song, X. Teng, Y. Liu, J. Wang, Y. Niu, X. He, C. Zhang, Z. Chen, Rational construction of self-supported triangle-like MOF-derived hollow (Ni,Co)Se_2 arrays for electrocatalysis and supercapacitors, Nanoscale, 11 (2019) 6401-6409.

[13] X. Wang, Y. Zheng, J. Yuan, J. Shen, J. Hu, A.-j. Wang, L. Wu, L. Niu, Porous NiCo Diselenide Nanosheets Arrayed on Carbon Cloth as Promising Advanced Catalysts Used in Water Splitting, Electrochim Acta, 225 (2017) 503-513.

[14] Q. Zhao, D. Zhong, L. Liu, D. Li, G. Hao, J. Li, Facile fabrication of robust 3D Fe–NiSe nanowires supported on nickel foam as a highly efficient, durable oxygen evolution catalyst, J Mater Chem A, 5 (2017) 14639-14645.

[15] H. Zhu, R. Jiang, X. Chen, Y. Chen, L. Wang, 3D nickel-cobalt diselenide nanonetwork for highly efficient oxygen evolution, Sci Bull, 62 (2017) 1373-1379.

[16] J. Li, H. Sun, L. Lv, Z. Li, X. Ao, C. Xu, Y. Li, C. Wang, Metal-Organic Framework-Derived Hierarchical (Co,Ni)Se_2@NiFe LDH Hollow Nanocages for Enhanced Oxygen Evolution, ACS Appl

Mater Interfaces, 11 (2019) 8106-8114.
[17] F. Zhang, Y. Pei, Y. Ge, H. Chu, S. Craig, P. Dong, J. Cao, P.M. Ajayan, M. Ye, J. Shen, Controlled Synthesis of Eutectic NiSe/Ni_3Se_2 Self-Supported on Ni Foam: An Excellent Bifunctional Electrocatalyst for Overall Water Splitting, Adv Mater Interfaces, 5 (2018).
[18] X. Hu, Q. Zhou, P. Cheng, S. Su, X. Wang, X. Gao, G. Zhou, Z. Zhang, J. Liu, Nickel-iron selenide polyhedral nanocrystal with optimized surface morphology as a high-performance bifunctional electrocatalyst for overall water splitting, Appl Surf Sci, 488 (2019) 326-334.
[19] J.-T. Ren, L. Chen, G.-G. Yuan, C.-C. Weng, Z.-Y. Yuan, Monolithic Ni_xM_y (M = OH, P, S, Se) nanosheets as efficient and stable electrocatalysts for overall water splitting, Electrochim Acta, 295 (2019) 148-156.
[20] B. Xu, H. Yang, L. Yuan, Y. Sun, Z. Chen, C. Li, Direct selenylation of mixed Ni/Fe metal-organic frameworks to NiFe-Se/C nanorods for overall water splitting, J Power Sources, 366 (2017) 193-199.
[21] Y. Zhao, G. Mao, Y. Du, G. Cheng, W. Luo, Colloidal Synthesis of NiWSe Nanosheets for Efficient Electrocatalytic Hydrogen Evolution Reaction in Alkaline Media, Chem Asian J, (2018).
[22] K. Xiao, L. Zhou, M. Shao, M. Wei, Fabrication of $(Ni,Co)_{0.85}Se$ nanosheet arrays derived from layered double hydroxides toward largely enhanced overall water splitting, J Mater Chem A, 6 (2018) 7585-7591.
[23] X. Li, X. Shang, X.-Y. Zhang, B. Dong, K.-L. Yan, Y.-R. Liu, G.-Q. Han, J.-Q. Chi, Y.-M. Chai, C.-G. Liu, Ni-Se nanostructrures dependent on different solvent as efficient electrocatalysts for hydrogen evolution reaction in alkaline media, Mater Chem Phys, 207 (2018) 389-395.
[24] S.-K. Park, J.K. Kim, Y. Chan Kang, Metal–organic framework-derived $CoSe_2$/$(NiCo)Se_2$ box-in-box hollow nanocubes with enhanced electrochemical properties for sodium-ion storage and hydrogen evolution, J Mater Chem A, 5 (2017) 18823-18830.
[25] K.S. Bhat, H.S. Nagaraja, Nickel selenide nanostructures as an electrocatalyst for hydrogen evolution reaction, Int J Hydrogen Energy, 43 (2018) 19851-19863.
[26] X. Zheng, X. Han, H. Liu, J. Chen, D. Fu, J. Wang, C. Zhong, Y. Deng, W. Hu, Controllable Synthesis of Ni_xSe ($0.5 \leq x \leq 1$) Nanocrystals for Efficient Rechargeable Zinc-Air Batteries and Water Splitting, ACS Appl Mater Interfaces, 10 (2018) 13675-13684.
[27] K. Ao, J. Dong, C. Fan, D. Wang, Y. Cai, D. Li, F. Huang, Q. Wei, Formation of Yolk–Shelled Nickel–Cobalt Selenide Dodecahedral Nanocages from Metal–Organic Frameworks for Efficient Hydrogen and Oxygen Evolution, ACS Sustain Chem Eng, 6 (2018) 10952-10959.
[28] C.L. McCarthy, C.A. Downes, R.L. Brutchey, Room Temperature Dissolution of Bulk Elemental Ni and Se for Solution Deposition of a $NiSe_2$ HER Electrocatalyst, Inorg Chem, 56 (2017) 10143-10146.
[29] F. Ming, H. Liang, H. Shi, G. Mei, X. Xu, Z. Wang, Hierarchical $(Ni,Co)Se_2$/Carbon Hollow Rhombic Dodecahedra Derived from Metal-Organic Frameworks for Efficient Water-Splitting Electrocatalysis, Electrochim Acta, 250 (2017) 167-173.
[30] X. Xu, H. Liang, F. Ming, Z. Qi, Y. Xie, Z. Wang, Prussian Blue Analogues Derived Penroseite $(Ni,Co)Se_2$ Nanocages Anchored on 3D Graphene Aerogel for Efficient Water Splitting, ACS Catal, 7 (2017) 6394-6399.
[31] Y. Chen, Z. Ren, H. Fu, X. Zhang, G. Tian, H. Fu, NiSe-$Ni_{0.85}$ Se Heterostructure Nanoflake Arrays on Carbon Paper as Efficient Electrocatalysts for Overall Water Splitting, Small, 14 (2018) 1800763.